Research Article | Vol. 27, No. 26 / 23 December 2019 / Optics Express 37579

Optics EXPRESS

Multimode photonic molecules for advanced force sensing

NICOLETTA GRANCHI,[1,2,*] MAURANGELO PETRUZZELLA,[3] DARIO BALESTRI,[1,2] ANDREA FIORE,[3] MASSIMO GURIOLI,[1] AND FRANCESCA INTONTI[1,2]

[1]*Dep. of Physics and Astronomy, University of Florence, via Sansone 1, I-50019 Sesto Fiorentino (FI), Italy*
[2]*European Laboratory for NonlinearSpectroscopy, via Nello Carrara 1, I-50019, Sesto Fiorentino (FI), Italy*
[3]*Dep. Applied Physics and Institute for Photonic Integration, Eindhoven University of Technology, 5600 MB Eindhoven, The Netherlands*
[*]*granchi@lens.unifi.it*

Abstract: We propose a force sensor, with optical detection, based on a reconfigurable multi-cavity photonic molecule distributed over two parallel photonic crystal membranes. The system spectral behaviour is described with an analytical model based on coupled mode theory and validated by finite difference time domain simulations. The deformation of the upper photonic crystal membrane, due to a localized vertical force, is monitored by the relative spectral positions of the photonic molecule resonances. The proposed system can act both as force sensor, with pico-newton sensitivity, able to identify the position where the force is applied, and as torque sensor able to measure the torsion of the membrane along two perpendicular directions.

1. Introduction

Among optical nano-resonators, photonic molecules, consisting of two or more interacting photonic crystal nano-cavities (PhCCs), represent an attractive platform for probing fundamental cavity quantum electrodynamics effects, for quantum information processing [1–4], and to realize an ultrabright source of entangled photon pairs [5]. Due to their ultranarrow resonances localized in diffraction limited dielectric volumes [6], PhCCs are strong candidates also for a new generation of devices for sensing and metrology applications [7–9]. Within this framework, the possibility to control the spectrum of a PhCC has been an active field of research in the last decade. The problem of the tuning of photonic modes has been addressed not only from a fundamental point of view, but also through cavity engineering [10] and through the development of post-fabrication techniques [11–15], quite often born in order to compensate fabrication induced disorder. Large mode tuning with minor reduction of quality factor Q has been recently demonstrated by the electromechanical control of the distance between two PhCCs realized on two closely spaced parallel membranes [16–18]. Specifically, the effects of a local force exerted by nanoscale mechanical and electro-mechanical actuation on reconfigurable bilayer photonic crystal resonators have been studied [19–20]. These actuation methods allow the control of the spectral properties of coupled cavities in an ultrawide spectral range, demonstrating a fine and reversible mode shift. Viceversa, by monitoring the variation of the coupling strength of the two PhCCs induced by the deformation of the upper membrane, forces can be measured with pico-Newton sensitivity [21].

So far these demonstrations involved the estimation of a point or quasi-uniform force, without discrimination of its spatial location and its extension to multiple point forces, which have important implications both for atomic force microscopy using parallel tips and for nano-particle measurement [22].

#378352 https://doi.org/10.1364/OE.27.037579
Journal © 2019 Received 18 Sep 2019; revised 12 Nov 2019; accepted 13 Nov 2019; published 12 Dec 2019

Optics EXPRESS

Here we propose a multimode mechanically-compliant device that can be exploited both as a spatially-selective force sensor and as a static 2D sensor. Its operating principle is based on the fact that a local force applied on flexible two-dimensional membrane produces a deformation dependent on the location of the force application point and on the mechanical constraints of the membrane. The resulting spatially-varying mechanical profile of the membrane can be transduced in the optical domain by measuring the spectral features of the coupled modes formed by N nanocavities patterned on this membrane and on a second reference membrane located below it. The full system comprising 2N coupled nanocavities located on this pair of membranes allows for the detection of both the variation of the intermembrane distance as well as the discrimination between different membrane curvatures. In our proposal, the structure is designed in order to exploit both the in-plane and out-of-plane couplings between the modes of N = 4 photonic cavities. In this regard, the possibility to design more than one nanocavity on each membrane makes the double membrane system very appealing also in the field of torque sensing along two orthogonal directions [23,24]. We intend to monitor this local deformation via the changes in the spectral features of the system which strongly depend on the local inter-membrane distance. The eight cavities distributed over the two membranes produce a pattern of 8 coupled modes whose spectra position acts as a bar code for the detection of the membrane deformation, which can be detected via a single spectral channel. The system is firstly studied from an analytical point of view, exploiting the coupled mode theory [25–28], in order to obtain a simple physical picture. Then, the results are validated by Finite Difference Time Domain (FDTD) simulations giving full and quantitative information about the coupled modes of the proposed sensor.

2. Analytical model and FDTD simulations

The photonic pattern of the investigated structure is sketched in Fig. 1(a). The planar design consists of four nanocavities realized by omitting 3 holes from a triangular photonic crystal lattice (L3 cavities). This pattern is realized on two parallel membranes. The analytical expression of the system is derived by considering multiple identical oscillators with resonant energy E_0, whose intra-membrane and inter-membrane couplings are mediated respectively by tunnelling rates g_i ($i = d,v,h$) and J_j ($j = 0,d,v,h$), assumed to be real. Here the label d, v and h denote the diagonal, vertical and horizontal interactions, respectively. These coupling constants are represented by the coloured arrows in Fig. 1(a), and depend on the reciprocal geometric orientation and position of the cavities. We assume zero detuning between the four in plane cavities. Temporal coupled mode theory can be used to explain the physical behaviour of double-membrane (DM) photonic structures [25–28]. When the inter-membrane distance d is small enough the out-of-plane evanescent field of one slab penetrates into the other, originating coupled modes that are vertically delocalized over the two membranes but inherit the in-plane symmetry of the original uncoupled modes.

The system can be described as an 8-dimensional eigenvalue problem. For sake of simplicity, hereafter we will use a ket-like notation for the eigenvector and the equation is then written in the form $M|\Psi) = E|\Psi)$. Note that the problem is fully classic and to avoid misunderstanding this is highlighted by the use of round parenthesis to close the ket-like symbol. On the basis of single cavity electric field-eigenfunctions $|i)$, we can expand the eigenvector as $|\Psi) = \sum_{i=1}^{8} c_i|i)$, where $i = 1...4$ ($i = 5...8$) are the fundamental modes of the single cavities of the top (bottom) membrane, and c_i are real coefficients. Due to the large spectral separation between the different modes of a single L3 cavity, we consider only the fundamental mode (Y1) of the four cavities.

The matrix of the eigenvalue problem is

$$M = \begin{pmatrix} A & B \\ B & A \end{pmatrix}$$

Optics EXPRESS

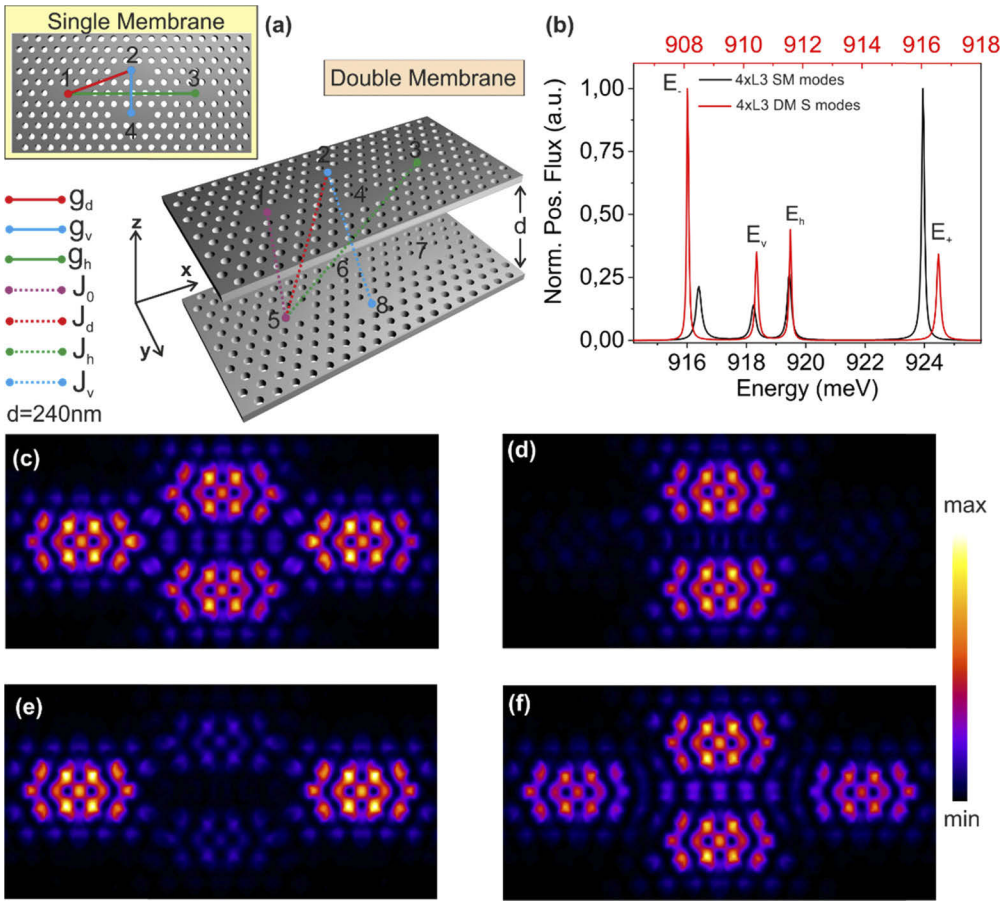

Fig. 1. **(a)** Sketch of the SM and DM 4xL3 system and the in-plane g_i (i = d,v,h) and out-of-plane J_j (j = 0,d,v,h) coupling factors. **(b)** FDTD spectra of the SM 4xL3 modes (black line) and of the DM 4xL3 S modes (red line). The electric field intensity maps of each mode -unvaried in the SM and DM configuration- are reported in increasing energy order (E_-, E_v, E_h, E_+) respectively in **(c)**, **(d)**, **(e)** and **(f)**. The suffixes represent the symmetry and spatial extension of the mode: h (v) means delocalization on the two horizontal (vertical) cavities, + (-) means complete delocalization on all the cavities at higher (lower) energy.

where $A = \begin{pmatrix} E_0 & g_d & g_h & g_d \\ g_d & E_0 & g_d & g_v \\ g_h & g_d & E_0 & g_d \\ g_d & g_v & g_d & E_0 \end{pmatrix}$ and $B = \begin{pmatrix} J_0 & J_d & J_h & J_d \\ J_d & J_0 & J_d & J_v \\ J_h & J_d & J_0 & J_d \\ J_d & J_v & J_d & J_0 \end{pmatrix}$ are the blocks that describe the in-plane and out-of plane interactions between the cavities, respectively. Notably, A is the matrix that, within this framework represents the eigenvalue problem of 4 coupled L3 cavities on a single membrane ((SM) 4xL3). The problem can be solved by calculating the eigenvalues and eigenvectors. Due to the vertical specular symmetry of the DM system, the photonic eigenstates split in symmetric (S, where $c_i = c_{i+4}$ i = 1...4) and antisymmetric (AS, where $c_i = -c_{i+4}$ i = 1...4)) modes, dividing the solutions into two separated symmetry classes.

Optics EXPRESS

The M matrix then becomes $M = \begin{pmatrix} M_+ & 0 \\ 0 & M_- \end{pmatrix}$, where

$$M_\pm = \begin{pmatrix} E_0 \pm \mathrm{J}_0 & g_d \pm \mathrm{J}_d & g_h \pm \mathrm{J}_h & g_d \pm \mathrm{J}_d \\ g_d \pm \mathrm{J}_d & E_0 \pm \mathrm{J}_0 & g_d \pm \mathrm{J}_d & g_v \pm \mathrm{J}_v \\ g_h \pm \mathrm{J}_h & g_d \pm \mathrm{J}_d & E_0 \pm \mathrm{J}_0 & g_d \pm \mathrm{J}_d \\ g_d \pm \mathrm{J}_d & g_v \pm \mathrm{J}_v & g_d \pm \mathrm{J}_d & E_0 \pm \mathrm{J}_0 \end{pmatrix} \tag{1}$$

This can be suitably read as a 4×4 matrix describing a single membrane 4xL3, where the uncoupled energy and tunnelling strength are:

$$\begin{aligned} E_0 &\rightarrow E_0 \pm \mathrm{J}_0 \\ g_d &\rightarrow G_d^\pm = g_d \pm \mathrm{J}_d \\ g_v &\rightarrow G_v^\pm = g_v \pm \mathrm{J}_v \\ g_h &\rightarrow G_h^\pm = g_h \pm \mathrm{J}_h \end{aligned} \tag{2}$$

$$M_\pm = \begin{pmatrix} E_0 \pm \mathrm{J}_0 & G_d^\pm & G_h^\pm & G_d^\pm \\ G_d^\pm & E_0 \pm \mathrm{J}_0 & G_d^\pm & G_v^\pm \\ G_h^\pm & G_d^\pm & E_0 \pm \mathrm{J}_0 & G_d^\pm \\ G_d^\pm & G_v^\pm & G_d^\pm & E_0 \pm \mathrm{J}_0 \end{pmatrix} \tag{3}$$

The eigenvalues are:

$$\begin{aligned} E_- &= \tfrac{1}{4}\left(2(E_0 \pm \mathrm{J}_0) + G_h^\pm + G_v^\pm - \sqrt{16(G_d^\pm)^2 + (G_h^\pm - G_v^\pm)^2}\right) \\ E_v &= E_0 \pm \mathrm{J}_0 - G_v^\pm \\ E_h &= E_0 \pm \mathrm{J}_0 - G_h^\pm \\ E_+ &= \tfrac{1}{4}\left(2(E_0 \pm \mathrm{J}_0) + G_h^\pm + G_v^\pm + \sqrt{16(G_d^\pm)^2 + (G_h^\pm - G_v^\pm)^2}\right) \end{aligned} \tag{4}$$

We therefore demonstrated that the spatial symmetry of the system allows describing the 8×8 problem with the same analytical expression of a single membrane 4xL3 structure. This also means that the variation of the intermembrane coupling can be mapped by the spectral and spatial distribution of the S and AS in-plane modes. This result is at the basis of our force and torque sensor proposal.

In order to estimate the in-plane (out-of-plane) coupling factors to be inserted in the matrix of Eq. (3), FDTD simulations were performed on single (double) membrane photonic molecules according to the required geometrical disposition. The investigated structures consist of single or double 200 nm thick GaAs (n = 3,484 in the spectral region of 1300 nm) slabs with triangular lattice (lattice constant a = 350 nm) and filling fraction f = 26%.

The inter-membrane distance at rest is $d = 240$ nm. In DM systems, the z-plane is a symmetry plane, and thus can be set to a perfect electric conductor or to perfect magnetic conductor depending whether anti-symmetric or symmetric modes are studied. In the simulated system the photonic modes were excited by a point-like dipole emitting at 1300 nm with a spectral broadening of 100 nm, placed at the centre of the left cavity. Figure 1(b) reports the spectrum

Optics EXPRESS

of the simulated SM 4xL3 (black line) and the spectrum of the symmetric modes of the DM 4xL3 (red line), acquired by a 5 µm x 3 µm sensor, placed 10 nm above the structure surface. In agreement with the coupling theory the S modes are located at lower energies than the corresponding single-membrane modes and they inherit the same spatial distributions as shown in Figs. 1(c)–1(f). The lowest energy mode (E_-) Fig. 1(c) and the highest energy mode (E_+) Fig. 1(f) are delocalized all over the 4 cavities, while the other two intermediate modes are mostly localized respectively in the vertical (E_v) Fig. 1(d) and horizontal cavities (E_h) Fig. 1(e). Not only the S modes exhibit a global redshift with respect to the SM resonances, they also present a larger splitting ($E_+ - E_-$), due to the composition of the in-plane and out-of-plane coupling factors [See Eq. (2) and Eq. (4)]. The AS modes (not shown in the figure) are located at higher energies with respect to the SM resonances, and consistently with Eq. (2) and Eq. (4) they present a reduction of the splitting ($E_+ - E_-$) of the order of 1 meV. The results of the coupled mode theory were exploited in order to calculate all the coupling factors by means of FDTD simulations. E_0 (920 meV) was extracted from the FDTD value of the energy of a single membrane L3 cavity fundamental mode [29]. Table 1 reports the calculated values of the in-plane coupling factors g_i (i = d,v,h), estimated for a SM 4xL3 structure, and the out-of-plane coupling factors J_j (j = 0,d,v,h) for the DM structures at d = 240 nm.

Table 1. Coupling Factors

g_d	g_v	g_h	J_0	J_d	J_v	J_h
−2.045 meV	1.101 meV	<10 µeV	8.959 meV	−0.279 meV	−0.042 meV	<10 µeV

Calculated values with FDTD simulations of the coupling terms between cavities according to the sketch of **Fig. 1(a)**.

Specifically, each (g_i) J_j coefficient was obtained by performing FDTD simulations on (single) double membrane photonic structures with the same nominal structural parameters in different configurations: (SM) DM 1xL3 for J_0, (SM) DM 2xL3 coupled diagonally, vertically and horizontally according to the geometry of the 4xL3 system, respectively to calculate (g_d) J_d, (g_v) J_v and (g_h) J_h. The signs of the coupling coefficients were attributed coherently with coupled modes basic theory [25–28]. We find the in-plane and out-of plane horizontal coupling to be negligible with respect to the other configurations. Moreover, coherently with the single L3 cavity fundamental mode spatial extension [29], the strongest interactions are given by g_d and J_0. The solutions of the simplified eigenvalue problem represented by the matrix (2) were numerically calculated by inserting the values of Table 1. For the analytical computation we disregard the coupling factors lower than 10 µeV (g_h and J_h). It was found that the analytical model provides an excellent toolbox for the comprehension of the investigated system. In Fig. 2(a) it is possible to appreciate the agreement between the FDTD energy values (blue dots) and the calculated eigenvalues (green triangles). The two data sets exhibit a systematic offset of the order of ≤1 meV, probably due to the approximations within the analytical model which considers independent the different couplings. For every energy peak we sketch the expected LDOS as predicted by the analytical model. Specifically we report the analytical intensity spatial profiles of the S modes, obtained by plotting bidimensional Gaussian functions with amplitudes equal to the relative weights $|c_i|^2 (i = 1 \ldots 4)$ of the eigenvectors on each cavity. This quantity represents the square modulus of the electric field, which can be linked to the expected LDOS. Notably from the comparison between Figs. 1(c)–1(f) and Figs. 2(b)–2(e), the calculated spatial profiles of the photonic molecule are in excellent agreement with the FDTD maps.

Optics EXPRESS

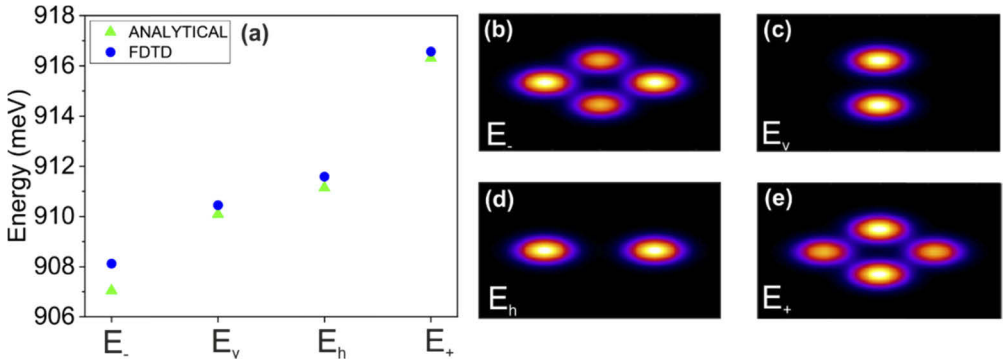

Fig. 2. **(a)** Comparison between the FDTD energy values of the S modes (blue dots) and the analytical S eigenvalues (green triangles) calculated by inserting the coupling factors of Table 1 in the matrix (2). The calculated intensity spatial profiles of the modes are reported in order of increasing energy (E_-, E_v, E_h, E_+) respectively in **(b)**, **(c)**, **(d)** and **(e)**. In order to visualize the mode extension, the analytical solutions were transformed in spatial maps obtained by plotting bidimensional Gaussians with amplitudes equal to the relative weights $|c_i|^2 (i = 1 \ldots 4)$ of the eigenvectors on each cavity.

3. Force and torque sensing

In this section we discuss how the proposed system can be employed as a torque and a force sensor. Specifically, leveraging on the spectral features detection from a single optical channel, the system is able to identify the position where the force is applied, with a sub-micrometer in-plane spatial resolution. It was experimentally proven that by reducing the intermembrane distance d, the molecular modes spectrally shift [19]. In particular the S modes shift to longer wavelengths, while the AS modes shift to shorter wavelengths. In these devices the coupling between the optical spectrum and the mechanical degree of freedom is realized by fabricating the upper crystal on a suspended microbridge. Specifically, the selected bridge geometry is composed of a rectangular photonic area (12 µm x 8 µm) connected to a supporting frame by four external microarms (2 µm x 2 µm) [16–18]. A sketch of the expected membrane deformation, after the application of a local vertical force F on one of the four L3 cavities, is reported in Fig. 3(a).

We analyzed the upper membrane vertical nano-deformation when a force is exerted at different xy positions on the top bridge. Given the in-plane symmetry of the photonic pattern, we focus on the mechanical actuation when the force is applied on two points: at the centre of the upper cavity and at the centre of the right cavity. Then, we monitor the membrane deformation along the x and y directions identified by the symmetry axes of the 4xL3 molecule. In order to relate the effect of a vertical local force to the deformation of the membrane in these two cases, a finite element method (FEM) algorithm is employed. An example of the simulated bending of the upper membrane for a local force of 2.5 µN acting on the right cavity is reported in Fig. 3(b). The frame at the top of Fig. 3(b) shows a horizontal cut of the FEM displacement map. This value of the force was chosen as it reproduces a maximum displacement of the upper membrane (the elastic constant of the dielectric membrane is k≈10 N/m) which is similar to the one obtained in the case of near-field mechanical actuation experiments on single cavities [19]. Using the deformation map we can determine the dependence of the out-of-plane coupling factors on the relative cavities z-coordinates by performing FDTD simulations on DM structures at different inter-membrane distances (from 240 nm to 80 nm in steps of 40 nm). In order to address the role of the upper membrane deformation in the entire system, from the FEM simulations of mechanical actuation on cavity 3 (2) we extract the dependence of the other 3 unperturbed cavities

Optics EXPRESS

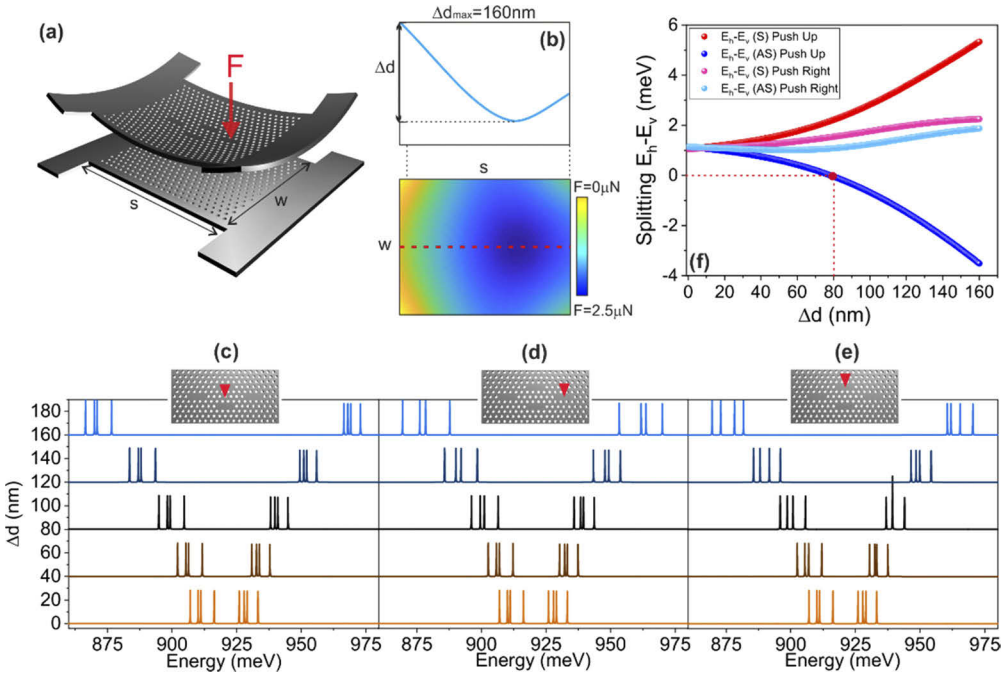

Fig. 3. **(a)** Sketch of the mechanical actuation on the DM 4xL3 system. **(b)** Results of a FEM simulation, in which we reproduce the elastic effect on the upper membrane (s = 5μm and w = 4μm) due to the actuation on the right cavity with a force of 2.5 μN. Similar results have been obtained for the actuation of the upper cavity. The bottom graphs report the trend of the S and AS modes analytical spectra in the three actuation regimes of interest: on the centre of the structure **(c)**, on the right cavity **(d)** and on the upper cavity **(e)**. Each far-field spectrum is calculated corresponding to a specific inter-membrane distance change, that varies from 0 nm (rest case) to 160 nm, and it is obtained by summing 4 Lorentzian functions with quality factor $Q = 10^4$ having a central wavelength equal to the calculated eigenvalues. **(f)** Energy splitting between the vertical and the horizontal modes E_v and E_h as a function of the intermembrane distance variation obtained by simulating the push on the right cavity (pink (S) and cyan (AS) dots) and on the upper cavity (red (S) and blue (AS) dots). The blue curve becomes zero when E_v and E_h cross for Δd = 78 nm.

z-coordinates, that is found to be directly proportional to the actuated cavity z-coordinate, i.e. Δd. With a linear fit we extract these proportionality coefficients.

Then J_j (Δd) in the matrix (3) is opportunely calculated for every cavity in each actuation step. For intermediate intermembrane distances, the J_j (Δd) values were obtained by polynomial interpolation of the FDTD-calculated values. Pushing the upper membrane at its centre does not significantly change the relative heights of each cavity with respect to the unperturbed case. Thus in this scenario the transformation (2) is still valid. The actuation on an off-centre point slightly breaks the vertical symmetry that leads to purely vertical S and AS modes. We tested the role in symmetry breaking evaluating the changes of the parameter $Gtest = (Jd_{1-6}\text{-}Jd_{5-2})/(Jd_{1-6}+Jd_{5-2})$, which turns out to be as small as $Gtest = 0.017$ when Δd varies from 0 to 160 nm, so the vertical symmetry breaking is negligible. This is also confirmed by the fact that since the variations of the in-plane spatial distributions are relatively more important than the variations of the out-of-plane distributions, as seen in FDTD calculated maps. This means that while c_1, c_2, c_3 and c_4 vary significantly with Δd with respect to the unperturbed case, we can still assume that $c_{k+4} \cong \pm c_k$ ($k = 1 \ldots 4$) for S/AS modes for every Δd. In other words, despite the symmetry breaking, we

Optics EXPRESS

can still use as a good approximation the picture of S and AS modes. We therefore consider the off-diagonal matrices B unchanged under the membrane deformation. This allows us to exploit the simplified eigenvalue problem for the feasibility study and it is confirmed by the fact that if we solve the eight-dimension and four-dimension eigenvalue problems (referring to the matrices M and $M_{\pm}$) by using the FDTD-calculated values, we find that the solutions coincide within the numerical accuracy of the simulations.

The analytical macroscopic far-field spectra of the S and AS modes as a function of the wavelength for different intermembrane separations are shown in the bottom panels of Fig. 3 for three different scenarios of actuation. We studied the effects of pushing on the centre of the pattern (Fig. 3(c)), on the right cavity (Fig. 3(d)) and on the upper cavity (Fig. 3(e)), as sketched on the top of each spectra panels. The analytical spectra are obtained by summing four Lorentzian functions with resonance energy centred in the solutions of the eigenvalue problem, and Q factor $Q = 10^4$, commonly achieved in modified L3 cavities [30]. Note that the variation of the intermembrane distance may vary the Q of the S and AS mode; we checked that this effect is not larger than 20% and we conclude that this has not an impact on our sensitivity and we neglected it. The first case (pushing in the center) exhibits no change in the spectral separation between the 4 symmetric modes and between the 4 anti-symmetric modes, as expected given the fact that the membranes remain parallel when the force is exerted at the centre of the upper structure. The other two insets clarify that mechanical actuation on right and upper cavities unambiguously induces very different spectral shifts of the coupled modes. In Fig. 3(f) we report, for the actuation on the right (pink and cyan dots) and on the upper (red and blue dots) cavity, the energy splitting between the vertical and the horizontal modes E_v and E_h for S and AS modes, respectively. By monitoring the energy splitting variations we find a striking evidence of the different system response to the effect of local forces acting on different points of the structure. In particular, this is highlighted by the AS E_v and E_h modes crossing at $\Delta d = 78$ nm, exhibited only when pushing on the upper cavity (as stressed by the red dashed lines in Fig. 3(f) and by the presence of three peaks in the spectrum of Fig. 3(e), third graph). The spectra in Figs. 3(c)-(e) highlight the sensitivity of the photonic LDOS to both the position of the force at the nanoscale and its strength. The structure of the spectra is indeed a kind of a 8 lines code bar for the upper membrane deformation. Note that the role of the in-plane coupling is just to split the 4 modes of each membrane. Accidentally two modes may spectrally coincide, as shown in Fig. 3(e), where the number of high energy modes go from four to three. In general, since the S and AS modes have different vertical distributions, and therefore different evanescent tails between the two membranes, they behave differently upon the membrane modification.

Figure 3 is intended for describing the working principle of the proposed system and for showing its entire dynamical range. While, for evaluating the sensitivity of the system we stress that by increasing Δd we find two actuation regimes, related to two different sensitivity parameters. The first regime is the *force sensing regime*, in which the S (AS) modes rigidly red (blue) shift, accordingly with the previous experimental results [19]**.** Here we can quantify the minimum detectable force (MDF) of the device, by evaluating the minimum detectable rigid shift of the modes, to be compared with a spectral resolution of the order of $\gamma/1000$ (where γ is the FWHM of a single peak with $Q = 10^4$) which can be detected by resonant detection methods [21]. Given the elastic constant (10 N/m) [18–21] of the membrane, we obtain a MDF of the order of 10 pN for a minimum displacement Δd of the order of 1 pm. For larger values of Δd the system enters in the *torque sensing regime*, in which the eight DM modes experiment a non-rigid shift with respect to one another, accompanied by a consequent modification of the energy splittings between the modes with respect to the initial condition. In other words, it is possible to distinguish between different force locations as soon as the 8 lines bar code changes configuration. Indeed a differentiation of the spectra at different xy coordinates of the force exertion show that mechanical actuation on right and upper cavities can be unambiguously

Optics EXPRESS

detected. We estimate the minimum detectable torque (MDT) by evaluating the minimum Δd for which it is possible to detect a variation of all the splittings $E_+ - E_h$, $E_h - E_v$ and $E_v - E_-$ with respect to the rest case. As the minimum Δd in this case results of the order of 0.03 nm, we find, with a calculation analogous to the case of MDF, that the MDT occurs for an applied force of the order of 0.3 nN (meaning a MDT of 2.6 10^{-14} Nm). We did not further investigate the maximum spatial resolution achievable with the proposed sensor since the current cavity design is optimized for torque-sensing. However from the data discussed above it is clear that we can distinguish when the force is applied on different cavities, which roughly gives a resolution in the range of 1 μm. Besides the spectral shift of the molecular modes due to a local pushing of the upper membrane, the molecular modes show also a modification of their spatial distribution. The predicted variation of the calculated intensity spatial profiles of the S modes is reported in Fig. 4. The method used to illustrate the spatial features of the modes is the same one of Fig. 2. For every resonance we follow the evolution of the near-field spatial features from the unperturbed case (Δd = 0 nm) (Fig. 4(a)) to the maximum push regime (Δd = 160 nm) on the right cavity (Fig. 4(b)) and on the upper cavity (Fig. 4(c)). A significant change in the distributions of the modes in the two regimes is found. From Figs. 4(b)–4(c) we also find that the fundamental mode E_- tends to localize on the pushed cavity (right in (b) and up in (c)), while the highest energy mode E_+ moves away from the actuated cavity. Specifically in the case (b) the E_- mode drift towards the opposite cavity (left). The spatial distribution of the vertical mode E_v (horizontal E_h) remains unchanged for actuation on the right (upper) cavity as it is substantially absent from it. The results reported in Fig. 4 show that by mapping the spatial distribution of the molecular modes

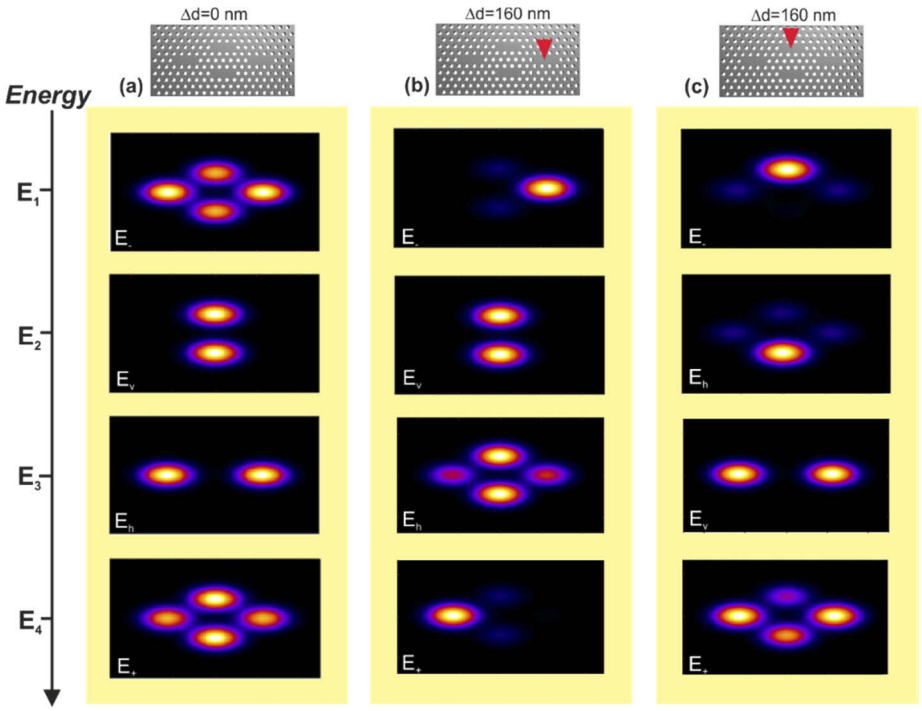

Fig. 4. Graphic representation of the calculated variation of the in-plane extension of the S modes (in order of increasing energy) for the unperturbed case (Δd = 0 nm) **(a)** and for extreme actuation on the right **(b)** and upper **(c)** cavity (Δd = 160 nm). The analytical maps were obtained by plotting bidimensional gaussians with amplitudes equal to the relative weights $|c_i|^2 (i = 1 \ldots 4)$ of the eigenvectors on each cavity in the different actuation regimes.

Optics EXPRESS

it is possible to monitor the intra membrane distance at different location in the xy plane. The presented approach can be therefore also employed as a tool for directly imaging the membrane deformation and can be potentially employed to map the vibration profiles of the mechanical modes of the upper membrane [31,32].

4. Conclusions

In conclusion, we have developed an analytical model that describes the physics of a multimode reconfigurable photonic molecule distributed over two parallel photonic crystal membranes. By employing the coupled modes theory, FEM and FDTD method simulations, we demonstrated that it is possible to characterize very different spectral responses of the investigated structure in two different mechanical actuation regimes, to be unambiguously related to the membrane deformation induced by the in-plane position of the force. This indicates that the investigated photonic molecule represents a promising platform for position sensitive force sensing with a spatial resolution in the range of 1 μm, and with a pico-newton force resolution, and for a torque sensor able to measure the torsion of the membrane along the two perpendicular directions. The resolution can be improved either increasing the cavity Q factor or modifying the elastic parameters of the suspending bridge. Finally, we showed that deformation imaging is achievable, and this could be exploited for mapping the vibrational modes of the membrane. We believe that these peculiar features would open the road to possible sensing applications within the framework of optoelectronics for force sensing applications.

Funding

Ente Cassa di Risparmio di Firenze (2016.0968).

Disclosures

The authors declare no conflicts of interest.

References

1. S. Noda, M. Fujita, and T. Asano, "Spontaneous-emission control by photonic crystals and nanocavities," Nat. Photonics **1**(8), 449–458 (2007).
2. D. Gerace, H. Türeci, A. Imamoglu, V. Giovannetti, and R. Fazio, "The quantum-optical Josephson interferometer," Nat. Phys. **5**(4), 281–284 (2009).
3. A. Majumdar, A. Rundquist, M. Bajcsy, V. D. Dasika, S. R. Bank, and J. Vuckovic, "Design and analysis of photonic crystal coupled cavity arrays for quantum simulation," Phys. Rev. B **86**(19), 195312 (2012).
4. R. Bose, T. Cai, K. R. Choudhury, G. S. Solomon, and E. Waks, "All-optical coherent control of vacuu, Rabi oscillations," Nat. Photonics **8**(11), 858–864 (2014).
5. A. Dousse, J. Suffczyński, A. Beveratos, O. Krebs, A. Lemaître, I. Sagnes, J. Bloch, P. Voisin, and P. Senellart, "Ultrabright source of entangled photon pairs," Nature **466**(7303), 217–220 (2010).
6. Y. Akahane, T. Asano, B. Song, and S. Noda, "High-*q* photonic nanocavity in a two-dimensional photonic crystal," Nature **425**(6961), 944–947 (2003).
7. A. Andueza, J. Pérez-Conde, and J. Sevilla, "Differential refractive index sensor based on photonic molecules and defect cavities," Opt. Express **24**(16), 18807–18816 (2016).
8. W. Lai, S. Chakravarty, Y. Zou, and R. T. Chen, "Silicon nano-membrane based photonic crystal microcavities for high sensitivity bio-sensing," Opt. Lett. **37**(7), 1208–1210 (2012).
9. M. Aspelmeyer, T. J. Kippenberg, and F. Maequardt, "Cavity Optomechanics," Rev. Mod. Phys. **86**(4), 1391–1452 (2014).
10. N. Caselli, F. Intonti, F. Riboli, and M. Gurioli, "Engineering the mode parity of the ground state in photonic crystal molecules," Opt. Express **22**(5), 4953–4959 (2014).
11. F. Intonti, S. Vignolini, F. Riboli, A. Vinattieri, D. S. Wiersma, M. Colocci, L. Balet, C. Monat, C. Zinoni, L. H. Li, R. Houdré, M. Francardi, A. Gerardino, A. Fiore, and M. Gurioli, "Spectral tuning and near-field imaging of photonic crystal microcavities," Phys. Rev. B **78**(4), 041401 (2008).
12. B. Cluzel, L. Lalouat, P. Velha, E. Picard, D. Peyrade, J. Rodier, T. Charvolin, P. Lalanne, F. de Fornel, and E. Hadji, "A near-field actuated optical nanocavity," Opt. Express **16**(1), 279–286 (2008).

Optics EXPRESS

13. F. Intonti, N. Caselli, S. Vignolini, F. Riboli, S. Kumar, A. Rastelli, O. Schmidt, M. Francardi, A. Gerardino, L. Balet, L. Li, A. Fiore, and M. Gurioli, "Mode tuning of photonic crystal nanocavities by photoinduced non thermal oxidation," Appl. Phys. Lett. **100**(3), 033116 (2012).
14. F. Intonti, S. Vignolini, F. Riboli, M. Zani, D. S. Wiersma, L. Balet, L. H. Li, M. Francardi, A. Gerardino, A. Fiore, and M. Gurioli, "Tuning of photonic crystal cavities by controlled removal of locally infiltrated water," Appl. Phys. Lett. **95**(17), 173112 (2009).
15. S. Vignolini, F. Intonti, L. Balet, M. Zani, F. Riboli, A. Vinattieri, D. S. Wiersma, M. Colocci, L. Li, M. Francardi, A. Gerardino, A. Fiore, and M. Gurioli, "Nonlinear optical tuning of photonic crystal microcavities by near-field probe," Appl. Phys. Lett. **93**(2), 023124 (2008).
16. L. Midolo, P. J. van Veldhoven, M. A. Dundar, R. Notzel, and A. Fiore, "Electromechanical wavelength tuning of double-membrane photonic crystal cavities," Appl. Phys. Lett. **98**(21), 211120 (2011).
17. L. Midolo, F. Pagliano, T. B. Hoang, T. Xia, F. W. M. van Otten, L. H. Li, E. H. Linfield, M. Lermer, S. Hofling, and A. Fiore, "Spontaneous emission control of single quantum dots by electromechanical tuning of a photonic crystal cavity," Appl. Phys. Lett. **101**(9), 091106 (2012).
18. M. Petruzzella, F. M. Pagliano, Ž Zobenica, S. Birindelli, M. Cotrufo, F. W. M. van Otten, R. W. van der Heijden, and A. Fiore, "Electrically driven quantum light emission in electromechanically tuneable photonic crystal cavities," Appl. Phys. Lett. **111**(25), 251101 (2017).
19. M. Petruzzella, F. La China, F. Intonti, N. Caselli, M. De Pas, F. W. M. van Otten, M. Gurioli, and A. Fiore, "Nanoscale mechanical actuation and near-field read-out of photonic crystal molecules," Phys. Rev. B **94**(11), 115413 (2016).
20. D. Balestri, M. Petruzzella, S. Checcucci, F. Intonti, N. Caselli, F. Sgrignuoli, F. W. M. van Otten, A. Fiore, and M. Gurioli, "Mechanical and electric control of photonic modes in random dielectrics," Adv. Mater. **31**(12), 1807274 (2019).
21. Z. Zobenica, R. W. van der Heijden, M. Petruzzella, F. Pagliano, R. Leijssen, T. Xia, L. Midolo, M. Cotrufo, Y. Cho, F. W. M. van Otten, E. Verhagen, and A. Fiore, "Integrated nano-opto-electro-mechanical sensor for spectrometry and nanometrology," Nat. Commun. **8**(1), 2216 (2017).
22. F. Liu, S. Alaie, Z. C. Leseman, and M. Hossein-Zadeh, "Sub-pg mass sensing and measurement with an optomechanical oscillator," Opt. Express **21**(17), 19555–19567 (2013).
23. J. P. Davis, D. Vick, D. C. Fortin, J. A. J. Burgess, W. K. Hiebert, and M. R. Freeman, "Nanotorsional resonator torque magnetometry," Appl. Phys. Lett. **96**(7), 072513 (2010).
24. M. Wu, A. C. Hryciw, C. Healey, D. P. Lake, H. Jayakumar, M. R. Freeman, J. P. Davis, and P. E. Barclay, "Dissipative and dispersive optomechanics in a nanocavity torque sensor," Phys. Rev. X **4**(2), 021052 (2014).
25. M. Bayer, T. Gutbrod, J. Reithmaier, A. Forchel, T. Reinecke, P. Knipp, A. Dremin, and V. Kulakovskii, "Optical Modes in Photonic Molecules," Phys. Rev. Lett. **81**(12), 2582–2585 (1998).
26. H. A. Haus, W.-P. Huang, S. Kawakami, and N. A. Whitaker, "Coupled-mode theory of optical waveguides," J. Lightwave Technol. **5**(1), 16–23 (1987).
27. N. Caselli, F. Riboli, F. La China, A. Gerardino, L. Li, E. H. Linfield, F. Pagliano, A. Fiore, F. Intonti, and M. Gurioli, "Tailoring the photon hopping by nearest-neighbor and next-nearest-neighbor interaction in photonic arrays," ACS Photonics **2**(5), 565–571 (2015).
28. D. Gerace and L. C. Andreani, "Low-loss guided modes in photonic crystal waveguides," Opt. Express **13**(13), 4939–4951 (2005).
29. A. R. A. Chalcraft, S. Lam, B. D. Jones, D. Szymanski, R. Oulton, A. C. T. Thijssen, M. S. Skolnick, D. M. Whittaker, T. F. Krauss, and A. M. Fox, "Mode structure of coupled L3 photonic crystal cavities," Opt. Express **19**(6), 5670–5675 (2011).
30. The model results are independent of the detailed cavity design.
31. E. Gavartin, R. Braive, I. Sagnes, O. Arcizet, A. Beveratos, T. J. Kippenberg, and I. Robert-Philip, "Optomechanical coupling in a two- dimensional photonic crystal defect cavity," Phys. Rev. Lett. **106**(20), 203902 (2011).
32. T. Antoni, A. G. Kuhn, T. Briant, P.-F. Cohadon, A. Heidmann, R. Braive, A. Beveratos, I. Abram, L. Le Gratiet, I. Sagnes, and I. Robert-Philip, "Deformable two-dimensional photonic crystal slab for cavity optomechanics," Opt. Lett. **36**(17), 3434–3436 (2011).